Hindawi
Advances in Materials Science and Engineering
Volume 2019, Article ID 9328630, 11 pages
https://doi.org/10.1155/2019/9328630

Research Article

Study on Constitutive Characteristic of As-Cast AA6061 Alloy under Plane Strain Compression Based on Orthogonal Analysis

Fangcheng Qin,[1,2] **Huiping Qi**,[3] **Yuehua Kang**,[1] **and Chongyu Liu**[2]

[1]*Guangdong Institute of Materials and Processing, Guangzhou 510650, China*
[2]*College of Materials Science and Engineering, Guilin University of Technology, Guilin 541004, China*
[3]*School of Materials Science and Engineering, Taiyuan University of Science and Technology, Taiyuan 030024, China*

Correspondence should be addressed to Huiping Qi; qhp9974@tyust.edu.cn

Received 17 March 2019; Revised 14 July 2019; Accepted 22 August 2019; Published 30 September 2019

Academic Editor: Ulrich Prahl

Copyright © 2019 Fangcheng Qin et al. This is an open access article distributed under the Creative Commons Attribution License, which permits unrestricted use, distribution, and reproduction in any medium, provided the original work is properly cited.

Constitutive relationship and microstructure evolution of as-cast AA6061 alloy were studied using plane strain compression (PSC) under the temperature of 300–450°C, the strain rate of 0.01–5 s^{-1}, and the strain of 0.9. It is found that the flow stress decreases with increasing temperature and decreasing strain rate. The dynamic recovery (DRV) and recrystallization (DRX) are found to easily occur by optical microscopic (OM) techniques. The softening mechanisms are mainly due to DRV that is accompanied by a slight DRX. Based on orthogonal analysis, the strain should be taken into account to derive the constitutive model accurately, and the interaction effect between the strain rate and temperature on the stress can be neglected when compared with the individual effect of the strain rate and temperature. The strain-compensated constitutive models based on orthogonal experiment are established, and the activation energy Q is found to be 158.465 kJ/mol. The correlation coefficient and the average absolute relative error between the experimental and the predicted results are 0.9946 and 4.2656%, respectively. The developed models can be used to predict the stress precisely at a wide range of strains, strain rates, and temperatures.

1. Introduction

AA6061 alloy is widely used in industries for the production of critical ring components in aerocraft, high-speed rail, and automobile due to its superior properties such as high-specific strength, excellent corrosion resistance, and sound weldability [1–3], and the hot ring rolling (HRR) is an advanced incremental forming technique to fabricate aluminium ring components [4, 5]. The thickness of the ring blank is gradually reduced with a progressively narrowing gap between the driving roll and idle roll during HRR, and the height of the ring is controlled by the axial rolls [6]. The ring blank experiences a complicated stress/strain state, which results in the flow behavior and microstructure evolution in the HRR that is different from those in the hot forging [7, 8]. Thus, the HRR is a complex-forming process with the characteristics of coupled thermomechanical effects, such as multipass, nonisothermal, and asymmetry deformation (plane strain compression).

It is widely reported that numerical investigation can provide a convenient way to study the microstructure evolution in the HRR by the combination of constitutive model, microstructure evolution model, and the finite element (FE) method than the experimental methods [9, 10]. As the macroreflection is related to the mechanisms of microscopic deformation and microstructure evolution, the flow behavior of the ring blank at elevated temperature is often characterized by the constitutive model [11]. However, the reliability of the numerical simulation heavily depends on how precisely the deformation behavior of the material is being represented by the constitutive model [12]. Therefore, it is critical to develop accurate constitutive model first. In the last few decades, some comprehensive reviews on constitutive modeling in hot working of metals and alloys could be found in international publications [13–16]. The constitutive

models are divided into three categories, including the phenomenological, physical-based, and artificial neural network (ANN) models, and their developments, prediction capabilities, and application scopes were introduced in detail, respectively [16]. Amongst the phenomenological constitutive models, the hyperbolic-sine law in an Arrhenius-type equation has been commonly used to derive the relationship of flow stress, strain rate, and temperature and also used as an input to numerical investigation for optimizing the process parameters [17–19]. Some studies [14, 15, 20] revealed that the strain does exert an important influence on the elevated temperature flow behavior for a wide range of metals and alloys. Thus, the modified Arrhenius-type model by the compensation of strain is developed to represent the flow behavior and deformation response of as-forged 42CrMo steel [21], modified 9Cr-1Mo ferritic steel [12, 22], and Al alloys [14] under specified loading conditions. Moreover, the orthogonal design and regression analysis are used to evaluate the significance of the influences of temperature, strain rate, and strain, as well as interaction between temperature and strain rate on flow behavior of TiNiNb and Ti17 alloys, and the results show that the effect of interaction between temperature and strain rate can be neglected in comparison with other factor [11, 19].

Until now, many research efforts mainly concentrate on the constitutive modeling in a hyperbolic-sine law of AA6061 alloy using uniaxial compression (UC) [23, 24], but studies associated with those in plane strain compression (PSC) condition are insufficient [25]. And the effect of strain on the material constants in constitutive modeling is also not analyzed by orthogonal experiment. The effect degree of the strain on the flow stress is still unclear. However, the reliability of the simulation results strongly depends on the constitutive model. Thus, the further studies on constitutive modeling are still required for a better understanding of these factors. In this study, the constitutive relationship and microstructure evolution of as-cast AA6061 alloy subjected to PSC were studied. Experimental stress-strain data carried out on a Gleeble-3500 thermal simulator were used to determine the material constants in these models, incorporating the effects of strain, strain rate, and temperature based on orthogonal experiment and regression analysis. The accuracy and reliability of these models for predicting the flow stress of the AA6061 alloy were evaluated.

2. Experimental Procedures

A commercial AA6061 alloy with the chemical composition (wt. %) of 0.67Si, 0.65Fe, 0.96Mg, 0.12Mn, 0.30Cu, 0.20Zn, 0.10Cr, 0.13Ti, and Al (balance) was used in this study. The AA6061 billet was produced by a continuous casting process. Then, a homogenized treatment at 823 K for 8 h was performed and slowly cooled to room temperature in air. The rectangular specimens with a length of 20 mm, width of 15 mm, and height of 10 mm for PSC were wire-cut from the as-homogenized billet. Isothermal compression tests were conducted using PSC techniques [8, 26]. The specimens were heated to 723 K at a heating rate of 5 K/s and soaked for 3 min. Subsequently, the specimens were cooled to the tested temperatures at 5 K/s and held for 1 min to eliminate the temperature gradient. The compression tests were carried out based on ASTM E209 standard using a Gleeble-3500 thermal simulator at temperatures of 573 K, 623 K, 673 K, and 723 K and strain rates of 0.01 s^{-1}, 0.1 s^{-1}, 1 s^{-1}, and 5 s^{-1}, respectively. A tantalum sheet with a thickness of 0.1 mm and graphite foil lubricant were used to reduce the friction between the specimens and the anvils. The specimens were compressed to a true strain of approximately 0.9. After tests, all specimens were quenched immediately in water to reserve deformed microstructure. The temperature and the load-stroke data were measured by K-type thermocouple. True stress-strain curves were converted automatically from the load-stroke data [19].

3. Results and Discussion

3.1. True Stress-Strain Curves. Figure 1 shows the true stress-strain curves of the AA6061 alloy under PSC [27]. It can be clearly seen that the stress increases with increasing strain rate at a constant temperature. It is mainly associated with the DRV and DRX that have not enough time to fully carry out at the high strain rate, whose softening effect cannot offset the hardening effect to some extent. Moreover, as the temperature increases, gradual decreases in stress can be found at a constant strain rate. This is simultaneously caused by the increase in the thermal activation and the decrease in the critical shear stress of crystal slip, and the obstructions of dislocation motion and crystal slip are reduced. The driving force of recrystallization increases, and then, the DRX accelerates and softening effect gradually increases [28, 29]. Importantly, the DRX is favorable for steady-state deformation by continuous stress softening and microstructure reconstitution [30]. Thus, the steady-state deformation is obtained because the competition between the work hardening effect and softening effect reaches to a dynamic balance.

It is worth noting that the stress-strain curves exhibit different characteristics under PSC. At lower strain rates ($\leq$1 s^{-1}), the stress decreases monotonically after the peak strain. It is mainly because the sufficient deformation time is given to dislocation motion and heat dissipation, leading to dynamic recovery or recrystallization. On the contrary, the dislocation density increases at higher strain rates, which results in an obvious work hardening. Moreover, the temperature has a clear effect on the degree of stress softening. For example, the softening degree is approximately 20 MPa at 573 K/0.01 s^{-1}, while it is only approximately 5 MPa at 723 K/0.01 s^{-1}, as shown in Figure 1(a). The results indicate that the stress at lower temperatures ($\leq$673 K) and lower strain rates ($\leq$1 s^{-1}) presents a higher softening compared with the other deformation conditions. Therefore, in this study, it was demonstrated that a continuous stress softening behavior plays a dominant role in PSC [27].

3.2. Microstructural Characterization. The microstructures of the AA6061 alloy under PSC are presented in Figure 2. The DRV mechanism is clarified with a high strain rate of 5 s^{-1}. At 400°C/5 s^{-1}, the microstructure is mainly characterized by the elongated grains and a large number of subgrains. The serrated boundaries are formed because of

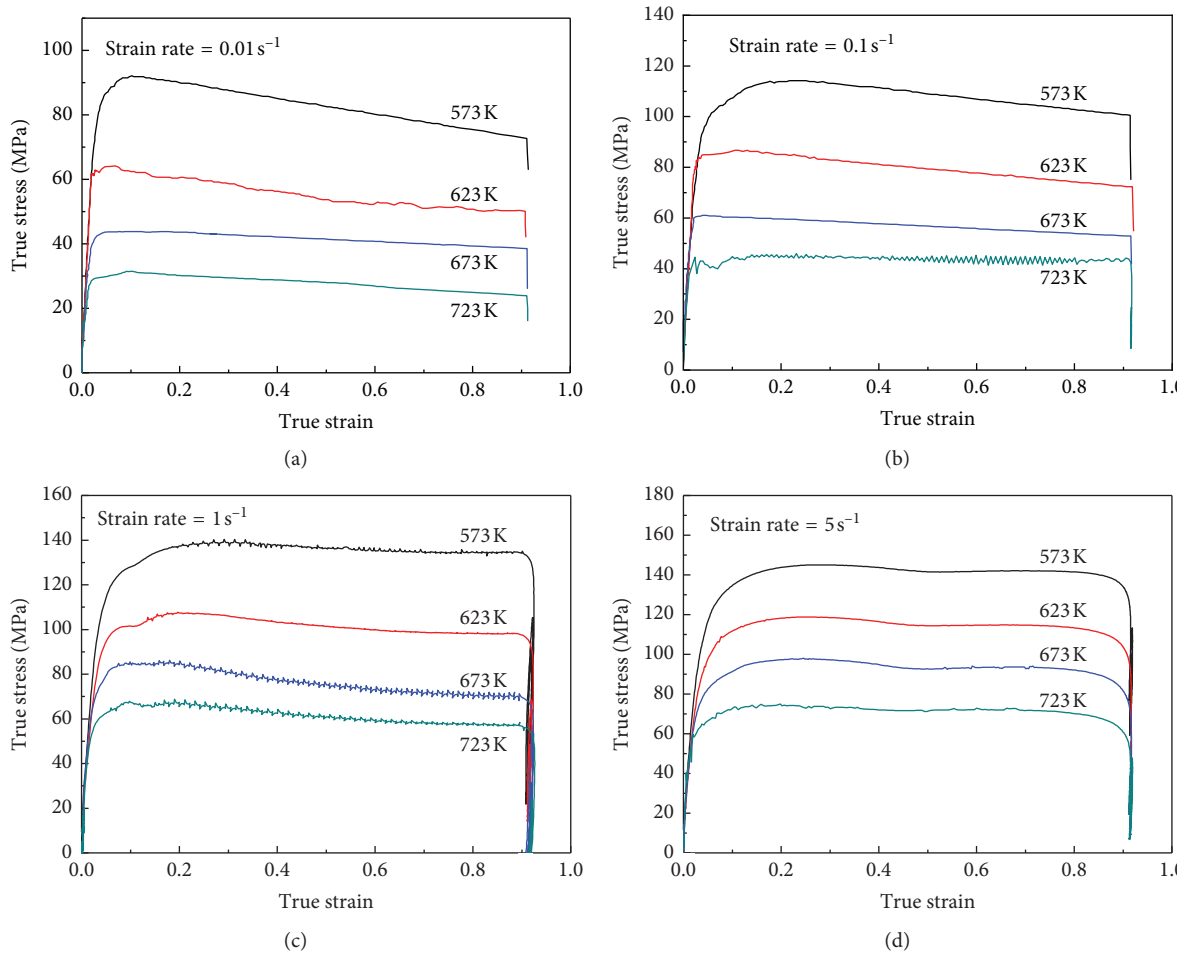

Figure 1: True stress-strain curves of the AA6061 under PSC with strain rates of (a) 0.01 s^{-1}; (b) 0.1 s^{-1}; (c) 1 s^{-1}; and (d) 5 s^{-1}.

the preferred recovery in the vicinity of grain boundaries, as shown in Figure 2(a). The presence of the serrated boundaries is an indication of the occurrence of extended the DRV [23]. Thus, it can be concluded that the driving force is not high enough to cause DRX, resulting in DRV. Also, the recrystallized grains are observed at 350°C/0.01 s^{-1}, and their average grain size and the volume fraction of the DRX increases as the temperature increases to 400°C. In Figures 2(b) and 2(c), the microstructures are characterized by the elongated grains with the nucleation of new fine grains along boundaries. Moreover, the recrystallized grains are also shown in Figure 2(c) with a low strain rate and high temperature. It can also be found that the subgrains decrease and the grain size increases. Thus, as the strain rate decreases and temperature increases, the DRX is enhanced. However, the degree of DRX is still low. The softening mechanisms in the AA6061 alloy after PSC are mainly due to DRV that is accompanied by a slight DRX.

3.3. Arrhenius-Type Constitutive Equations. The relationship among the flow stress, strain rate, and temperature at a constant strain can be expressed as the Arrhenius-type equation proposed by Sellars and McTegart [31]. Besides, the Zener–Hollomon (Z) parameter can be used to describe the effects of the temperature and strain rate on the flow stress [32, 33]:

$$Z = \dot{\varepsilon} \exp\left(\frac{Q}{RT}\right) = F_1(\sigma) = A_1 \sigma^{n_1}, \quad (1)$$

$$Z = F_2(\sigma) = A_2 \exp(\beta\sigma), \quad (2)$$

$$Z = F(\sigma) = A[\sinh(\alpha\sigma)]^n, \quad (3)$$

where σ is the flow stress (MPa); $\dot{\varepsilon}$ is the strain rate (s^{-1}); Q is the activation energy (kJ/mol); T is the absolute temperature (K); R is the universal gas constant (8.314 J/mol·K); A, A_1, A_2, β, and α are material constants; n and n_1 are the stress exponents; and α can be calculated as $\alpha = \beta/n_1$.

The power law equation (1) and exponent-type equation (2) are suitable for a low stress level ($\alpha\sigma < 0.8$) and high stress level ($\alpha\sigma > 1.2$), respectively. The hyperbolic-sine law, equation (3), is a more general form suitable for all stress level.

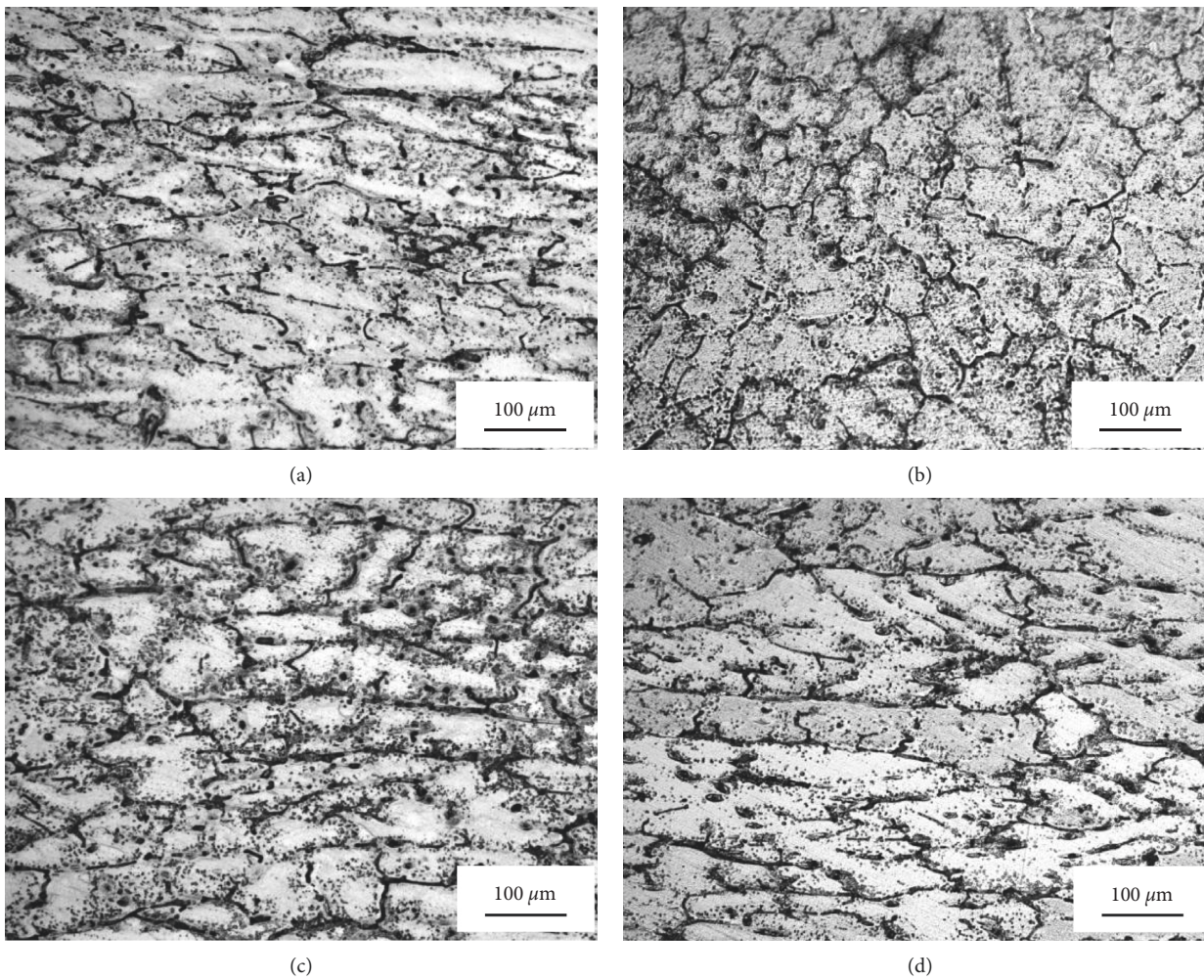

Figure 2: Microstructures of the AA6061 alloy after PSC under different conditions: (a) 400°C/5 s^{-1}; (b) 350°C/0.01 s^{-1}; (c) 400°C/0.01 s^{-1}; and (d) 300°C/5 s^{-1}.

According to equations (1) and (2), the β and n_1 are taken as the average values of the slopes in the $\ln\dot{\varepsilon}$ vs. σ plots and $\ln\dot{\varepsilon}$ vs. $\ln\sigma$ plots, respectively, at a series of temperatures.

Thus, for all stress level, the following relationship between strain rate and stress can be derived by substituting equation (1) into equation (3):

$$\dot{\varepsilon} = A \cdot [\sinh(\alpha\sigma)]^n \exp\left[\frac{-Q}{RT}\right]. \tag{4}$$

To obtain the values of the n and Q, the natural logarithm and partial differential of both sides of equation (4) are taken as follows:

$$\ln\sinh(\alpha\sigma) = \frac{1}{n}\ln\dot{\varepsilon} + \frac{Q}{nRT} - \frac{1}{n}\ln A, \tag{5}$$

$$Q = R\left[\frac{\partial\ln\dot{\varepsilon}}{\partial\ln[\sinh(\alpha\sigma)]}\right]_T \cdot \left[\frac{\partial\ln[\sinh(\alpha\sigma)]}{\partial(1/T)}\right]_{\dot{\varepsilon}} = RnS. \tag{6}$$

Combining with the true stress-strain curves, the n and Q can be evaluated using equations (5) and (6). The n is the average slope of $\ln\dot{\varepsilon}$ vs. $\ln[\sinh(\alpha\sigma)]$ plots at different temperatures, and S is the average slope of $\ln[\sinh(\alpha\sigma)]$ vs. $(1/T)$ plots at different strain rates. In this study, the peak stresses are used to calculate the required material constants. The plots to determine the average values of β, n_1, n, and S for PSC are presented in Figures 3(a)–3(d), respectively [27].

Additionally, taking the natural logarithm of both sides of equation (3), the value of A can be expressed as follows:

$$\ln Z = \ln A + n\ln\sinh(\alpha\sigma). \tag{7}$$

By substituting the $\ln Z$ values into equation (7), the A value can be calculated. The material constants are listed in Table 1, and equation (8) is the Arrhenius-type constitutive models for the AA6061 alloy under PSC with the activation energy Q of 175.836 kJ/mol. The Q is an important parameter serving as an indicator of difficulty degree in plasticity deformation, which is closely related to deformation mode in addition to alloy content and heat treatment [32, 34–36].

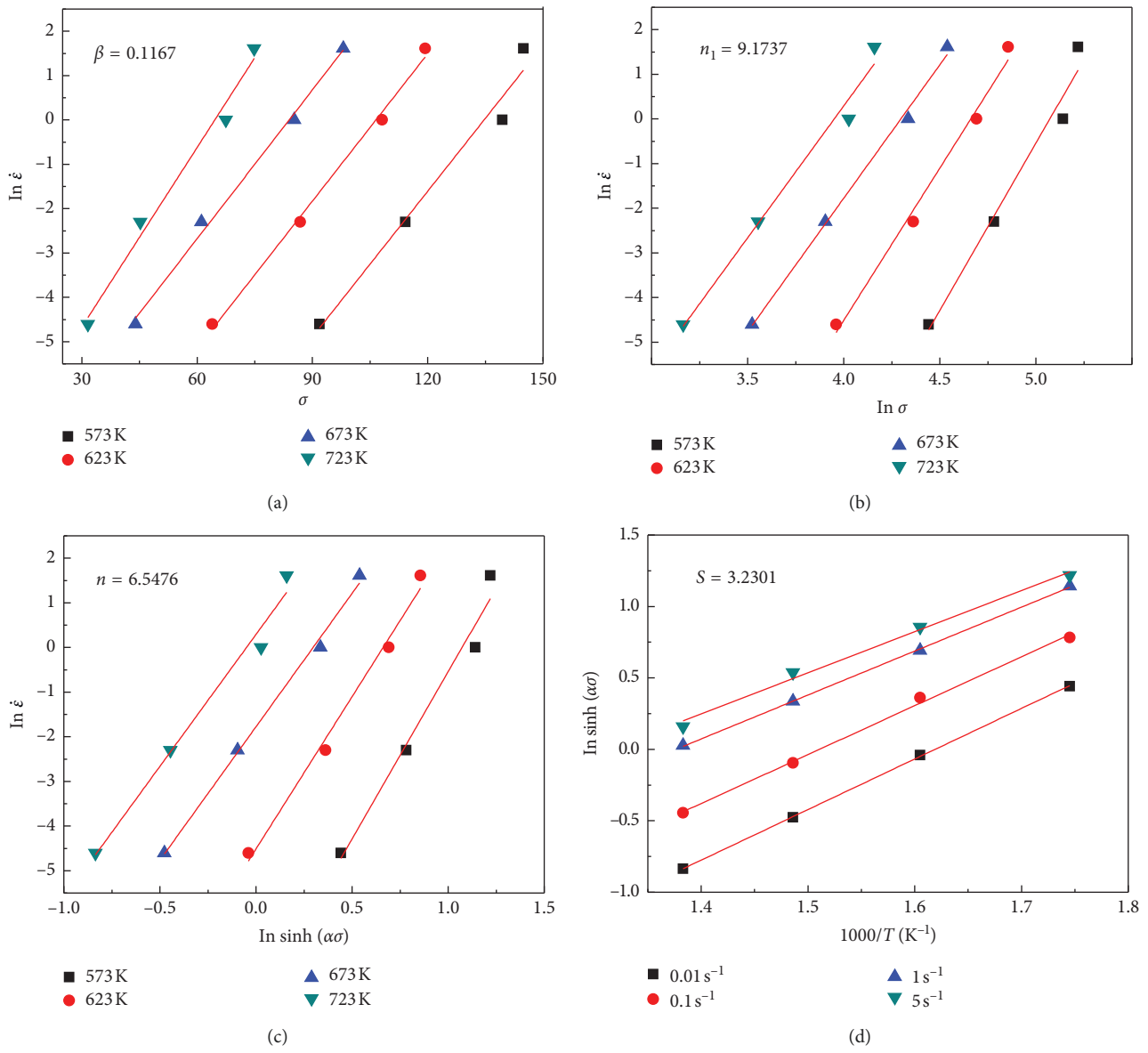

Figure 3: Relationships between (a) $\ln \dot{\varepsilon}$-σ; (b) $\ln \dot{\varepsilon}$-lnσ; (c) $\ln \dot{\varepsilon}$-ln$[\sinh(\alpha\sigma)]$; and (d) $\ln[\sinh(\alpha\sigma)]$-$(1/T)$ for PSC.

Table 1: Values of material constants of the AA6061 alloy under PSC [27].

Conditions	A (s^{-1})	β	n_1	α (MPa^{-1})	n	Q (kJ/mol)
PSC	7.06×10^{12}	0.1167	9.1737	0.01272	6.5476	175.836

$$\dot{\varepsilon} = 7.06 \times 10^{12} \cdot [\sinh(0.01272\sigma)]^{6.5476} \exp\left[\frac{-175836}{RT}\right]. \quad (8)$$

3.4. Constitutive Models Based on Orthogonal Analysis

3.4.1. Orthogonal Analysis. It is generally reported that the effect of the strain on flow behavior is unconspicuous, and thereby not considered in constitutive modeling [22, 37, 38]. In addition, some studies revealed that the materials constants in the Arrhenius-type constitutive equations varied with the strain, and the modified constitutive models by compensation of strain are proposed [14, 15, 20]. However, the influence degree of the strain on the flow stress of the AA6061 alloy is still unclear.

To estimate the effect of the strain rate, temperature, strain, and interaction between the strain rate and temperature on the flow stress, some values of the stress related to the relevant conditions under PSC shown in Table 2 are introduced to the orthogonal experiment. An orthogonal test table (L32 $(8^1 * 4^8)$) is used to present the influence

Table 2: The list of factors of the AA6061 alloy under PSC.

Level	Factor		
	A	B	C
	ε	$\dot{\varepsilon}$ (s^{-1})	T (K)
1	0.1	0.01	573
2	0.2	0.1	623
3	0.3	1	673
4	0.4	5	723
5	0.5		
6	0.6		
7	0.7		
8	0.8		

Table 3: Experimental program of orthogonal analysis with mixed levels.

Test no.	Column									Stress (MPa)
	A	B				C	B ∗ C			
	1	2	3	4	5	6	7	8	9	
1	1	1	1	1	1	1	1	1	1	92.106
2	1	2	2	2	2	2	2	2	2	86.683
3	1	3	3	3	3	3	3	3	3	84.875
4	1	4	4	4	4	4	4	4	4	72.783
5	2	1	3	1	4	2	4	2	3	60.654
6	2	2	4	2	3	1	3	1	4	113.89
7	2	3	1	3	2	4	2	4	1	66.77
8	2	4	2	4	1	3	1	3	2	97.32
9	3	1	2	2	3	4	4	3	1	29.83
10	3	2	1	1	4	3	3	4	2	59.152
11	3	3	4	4	1	2	2	1	3	107.02
12	3	4	3	3	2	1	1	2	4	144.93
13	4	1	4	2	2	3	1	4	3	42.754
14	4	2	3	1	1	4	2	3	4	44.685
15	4	3	2	4	4	1	3	2	1	138.81
16	4	4	1	3	3	2	4	1	2	118.49
17	5	1	3	4	2	4	3	1	2	29.152
18	5	2	4	3	1	3	4	2	1	58.135
19	5	3	1	2	4	2	1	3	4	104.59
20	5	4	2	1	3	1	2	4	3	144.58
21	6	1	1	4	3	3	2	2	4	37.167
22	6	2	2	3	4	4	1	1	3	43.508
23	6	3	3	2	1	1	4	4	2	137.93
24	6	4	4	1	2	2	3	3	1	116.47
25	7	1	4	3	4	1	2	3	2	82.518
26	7	2	3	4	3	2	1	4	1	79.322
27	7	3	2	1	2	3	4	1	4	75.143
28	7	4	1	2	1	4	3	2	3	71.704
29	8	1	2	3	1	2	3	4	4	52.937
30	8	2	1	4	2	1	4	3	3	106.65
31	8	3	4	1	3	4	1	2	2	59.224
32	8	4	3	2	4	3	2	1	1	93.311

factors and the experimental program of orthogonal analysis, as given in Tables 2 and 3. In addition, Table 3 also provides the stress values, and it will be regarded as objective function to estimate the significance of those factors. Table 4 indicates the calculated results about PSC of the AA6061 alloy, respectively. In the above tables, SS is the sum of squares of deviations; df is the degree of freedom; MS is the average value of squares of deviations that is equal to SS divided by the corresponding df; F is the f-distribution in Mathematic Statistic, which is used to evaluate the significance of each influence factor on the stress.

Table 4: ANOVA (analysis of variance) table of the AA6061 alloy under PSC.

Source	SS	df	MS	F	Sig.
A	37763.21	7	5394.74	22.362	**
B	73465.94	3	24488.65	168.357	***
C	253116.08	3	84372.03	324.661	***
B ∗ C	7049.674	9	783.29	9.06	*
Error	4064.862	9	451.65		
Total	375459.766	31			

In Table 4, the stresses of the AA6061 alloy under PSC are extremely sensitive to the temperature and strain rate. Moreover, it is worth noting that the strain has an influence on the stress that cannot be neglected with F about 22.362. However, the interaction effect between the strain rate and temperature on the stress with F of 9.06 can be neglected when compared with the individual effect of the strain rate and temperature.

3.4.2. Contribution Functions and Constitutive Models. It can be concluded from the results of orthogonal analysis that the strain also should be taken into account to derive the constitutive model accurately. In order to construct the model considering the effect of temperature, strain rate, and strain on the stress, some values of the stress at the temperature (573 K, 623 K, 673 K, and 723 K), strain rate ($0.01\ s^{-1}$, $0.1\ s^{-1}$, $1\ s^{-1}$, and $5\ s^{-1}$), and strain (0.1, 0.15, 0.2, 0.25, 0.3, 0.35, 0.4, 0.45, 0.5, 0.55, 0.6, 0.65, 0.7, 0.75, and 0.8) were used to make regression analysis.

The average values of the selected stress for as-cast AA6061 alloy in PSC with the same temperature, strain rate, or strain could be calculated by the following equation:

$$\overline{\sigma} = \sum_{x} \frac{\sigma(\varepsilon, \dot{\varepsilon}, T)}{n}, \tag{9}$$

where $\overline{\sigma}$ is the average value of the selected stress; $\sigma(\varepsilon, \dot{\varepsilon}, T)$ is the stress corresponding to the deformation parameters; x is the variables; and n is the number of the factors. For instance, the stress 79.476 MPa is calculated by averaging all the selected stress values under the same strain of 0.3. Thus, the average values of the AA6061 alloy given in Table 5 can be used to make regression analysis to derive the constitutive models concerning the temperature, strain rate, and strain.

According to Figure 4(a), a polynomial function about the stress and strain of the AA6061 alloy can be expressed as follows:

$$\sigma = -339.95\varepsilon^4 + 676.81\varepsilon^3 - 468.03\varepsilon^2 + 118.36\varepsilon + 70.66. \tag{10}$$

The relationship between the stress and strain rate plotted in Figure 4(b) is given as follows:

$$\ln\sigma = 4.4748 + 0.1149\ln\dot{\varepsilon}. \tag{11}$$

Table 5: Average values of the flow stress of the AA6061 alloy.

Strain	Stress (MPa)	Strain rate (s^{-1})	Stress (MPa)	Temperature (K)	Stress (MPa)
0.1	78.458	0.01	51.713	573	119.693
0.15	79.913	0.1	68.875	623	89.767
0.2	80.548	1	90.926	673	68.734
0.25	80.244	5	102.06	723	52.356
0.3	79.476				
0.35	78.696				
0.4	77.759				
0.45	76.864				
0.5	76.083				
0.55	75.754				
0.6	75.279				
0.65	75.036				
0.7	74.701				
0.75	74.132				
0.8	73.092				

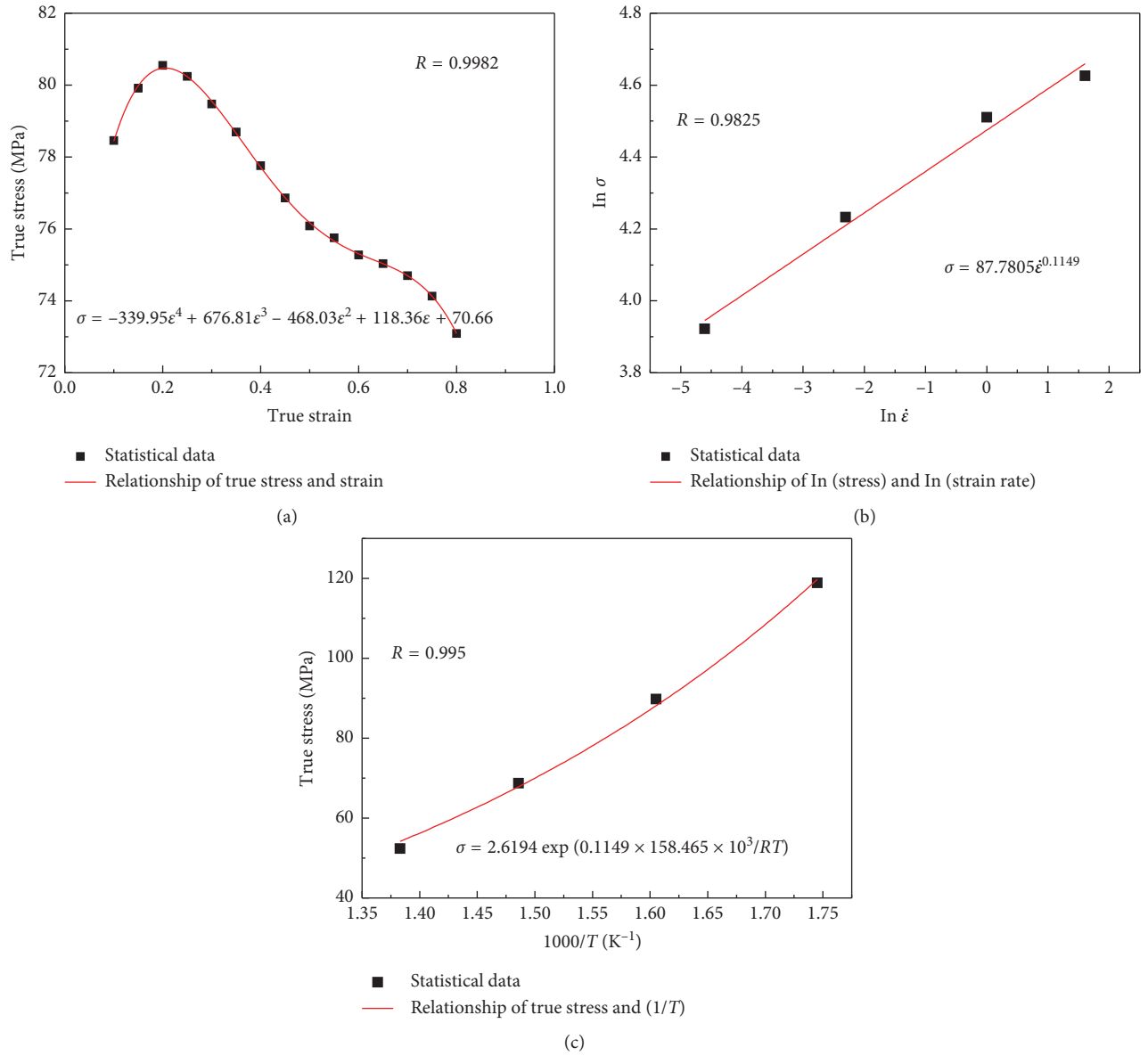

Figure 4: Correlation between (a) true stress and strain; (b) ln (true stress) and ln (strain rate); and (c) true stress and 1000/T under PSC conditions.

Taking exponentiation of both sides of equation (11) gives

$$\sigma = 87.7805\dot{\varepsilon}^{0.1149}. \tag{12}$$

Equation (12) represents that the average values of the strain rate sensitivity exponent m for the AA6061 alloy in PSC is 0.1149, respectively.

The relationship between the stress and temperature plotted in Figure 4(c) is given as

$$\sigma = 2.6194\exp\left(\frac{2190}{T}\right) = 2.6194\exp\left(\frac{0.1149\times 158.465\times 10^3}{RT}\right), \tag{13}$$

in which T is the absolute temperature (K); R is the universal gas constant (8.314 J/mol·K); the activation energy Q for as-cast AA6061 alloy can be found to be 158.465 kJ/mol, which are close to the value of as-forged AA6061 alloy acquired by [39, 40]. It is worth noting that the Q value based on orthogonal design is different from that presented in Table 1, and the effects of the strain on material constants are neglected in the Arrhenius-type constitutive equation.

Based on the results of orthogonal analysis, the strain should be taken into account to derive the constitutive model, and the interaction effect between the strain rate and temperature on the stress can be neglected. Moreover, the chemical composition does not change during hot deformation, and the microstructure evolution is also consistent with deformation parameters. Thus, the influence of the temperature, strain rate, and strain on the stress is independent, and the constitutive relationship of the AA6061 alloy can be expressed as follows [11, 19]:

$$\sigma = \sigma(\varepsilon, \dot{\varepsilon}, T), \tag{14}$$

$$\sigma = \sigma_0 \cdot f_\varepsilon \cdot f_{\dot{\varepsilon}} \cdot f_T, \tag{15}$$

where ε is the strain; $\dot{\varepsilon}$ is the strain rate; T is the absolute temperature (K); σ_0 is the initial stress of as-cast AA6061 alloy in PSC conditions; and f_ε, $f_{\dot{\varepsilon}}$, and f_T are the contribution factors or influence factors of the strain, strain rate, and temperature, respectively.

Importantly, the contribution factors should satisfy the following equation:

$$1 + \frac{\Delta\sigma}{\sigma_0} = f_\varepsilon \cdot f_{\dot{\varepsilon}} \cdot f_T. \tag{16}$$

In equation (16), $\Delta\sigma$ is the increment with regard to the initial stress, $\Delta\sigma = \sigma - \sigma_0$.

In this study, the average values of the stress corresponding to the minimum value of the selected strain, strain rate, and temperature in Table 5 should be regarded as the initial stress in accordance with equations (10)–(13), respectively. Therefore, the initial stress value σ_0 of the AA6061 alloy is calculated as 83.28 MPa. In addition, the calculation formulas of the contribution factors f_ε, $f_{\dot{\varepsilon}}$, and f_T for the AA6061 alloy can be obtained by equations (10), (12), and (13), respectively, through unitary processing according to the starting value. For instance, the initial contribution value of f_ε can be determined by inserting the minimum value of the selected strain 0.1 into equation (10). The calculation formulas of the contribution factors f_ε, $f_{\dot{\varepsilon}}$, and f_T for the AA6061 alloy are described as follows:

$$\begin{aligned} f_\varepsilon &= -4.3327\varepsilon^4 + 8.6261\varepsilon^3 - 5.9652\varepsilon^2 + 1.5085\varepsilon + 0.9005, \\ f_{\dot{\varepsilon}} &= 1.6975\dot{\varepsilon}^{0.1149}, \\ f_T &= 0.02188\exp\left(\frac{0.1149\times 158.465\times 10^3}{RT}\right). \end{aligned} \tag{17}$$

By substitution of f_ε, $f_{\dot{\varepsilon}}$, and f_T into equation (15), a novel constitutive model based on orthogonal analysis can be developed. Moreover, the effect of both the temperature and strain rate on the flow stress could be described by the Zener–Hollomon parameter (Z), which is defined as $Z = \dot{\varepsilon}\exp(Q/RT)$, and thereby the developed constitutive model of the AA6061 alloy can be represented as follows:

$$\begin{aligned} \sigma = 3.0931\big(&-4.3327\varepsilon^4 + 8.6261\varepsilon^3 - 5.9652\varepsilon^2 \\ &+ 1.5085\varepsilon + 0.9005\big)Z^{0.1149}. \end{aligned} \tag{18}$$

3.4.3. Verification of Constitutive Models Based on Orthogonal Analysis. A comparison between the experimental and the predicted flow stress is conducted to verify the accuracy of the above-developed constitutive models based on orthogonal analysis. Figure 5 shows the detailed comparisons of the experimental flow stress and the predicted flow stress of the AA6061 alloy under PSC. It can be found that the predicted stress could agree well with the experimental stress throughout the entire strain range toward the compression conditions. The predicted stresses increase with the decrease in temperature and the increase in strain rate, which satisfy the experimental one. Only in the conditions at 573 K with $1\,s^{-1}$ and $5\,s^{-1}$ for the AA6061 alloy, a slight difference between the predicted results and experimental results could be discovered. Both the experimental and predicted results reveal that the softening effect plays a dominant role after peak strain [41, 42]. Some researchers found that the stress is lower at low strain rate and high temperature, and thus, the DRX is more likely to occur, leading to a considerable grain refinement [43, 44]. Figures 2 and 5 demonstrate that the developed constitutive models can fit this conclusion well.

In this study, the correlation coefficient (R) and average absolute relative error (AARE) are used to evaluate the correlation between the experimental results and the predicted results of the flow stress under all testing conditions. They are expressed as follows [11, 22]:

$$\begin{aligned} R &= \frac{\sum_{i=1}^{N}\left(\sigma_e^i - \overline{\sigma}_e\right)\left(\sigma_p^i - \overline{\sigma}_p\right)}{\sqrt{\sum_{i=1}^{N}\left(\sigma_e^i - \overline{\sigma}_e\right)^2\sum_{i=1}^{N}\left(\sigma_p^i - \overline{\sigma}_p\right)^2}}, \\ \mathrm{AARE}(\%) &= \frac{1}{N}\sum_{i-1}^{N}\left|\frac{\sigma_e^i - \sigma_p^i}{\sigma_e^i}\right| \times 100, \end{aligned} \tag{19}$$

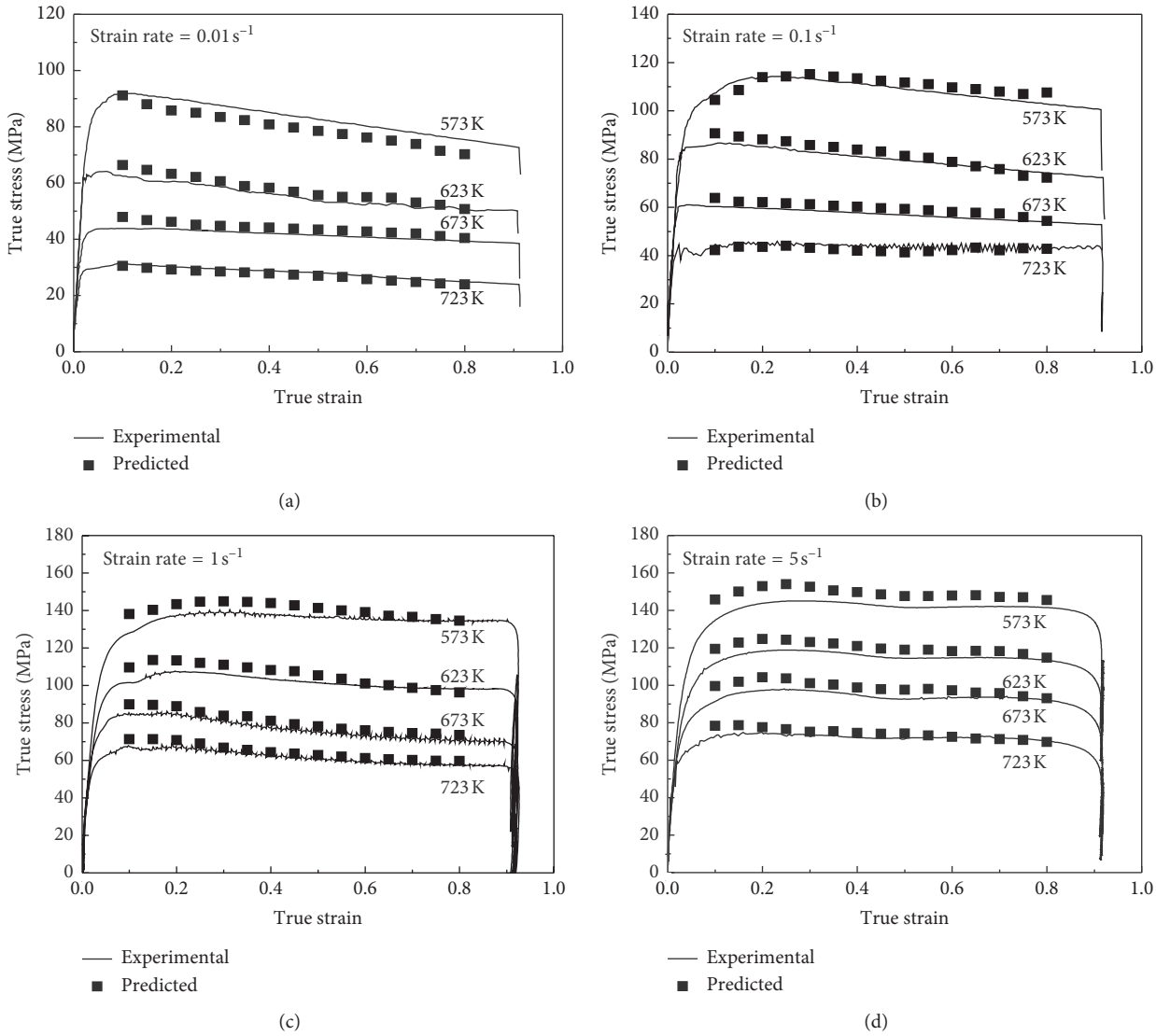

Figure 5: Comparisons of the experimental and the predicted flow stress from the constitutive models based on orthogonal analysis under PSC conditions.

where σ_e is the experimental flow stress; σ_p is the predicted flow stress from the developed constitutive model; $\overline{\sigma}_e$ and $\overline{\sigma}_p$ are the average values of σ_e and σ_p, respectively; and N is the total number of the selected flow stress data in this study.

As indicated in Figure 6, the $R = 0.9946$ and AARE = 4.2656% between the experimental and the predicted flow stress are obtained for as-cast AA6061 alloy, respectively. However, it should be noted that the higher value of R does not always imply a better correlation because the above equation tends to be partial usually to higher or lower values. Thus, the AARE as an impartial parameter is calculated for estimating the reliability of the developed models in prediction of the flow stress. From Figure 6, they reflect the excellent predictability of the developed models, which can be used as an input in the finite element analysis to obtain the flow stress at a wide range of strains, strain rates, and temperatures useful for predicting the flow localization or fracture during the HRR of the AA6061 alloy.

4. Conclusions

The constitutive relationship and microstructure evolution of the AA6061 alloy were studied by PSC in the temperature of 300–450°C, the strain rate of 0.01–5 s^{-1}, and the strain of 0.9. The main conclusions as follows:

(1) The flow stress decreases with increasing temperature and decreasing strain rate. The softening mechanisms in the AA6061 alloy after PSC are mainly due to DRV that is accompanied by a slight DRX.

(2) Based on the results of orthogonal analysis, the strain should be taken into account to derive the constitutive model accurately, and the interaction effect

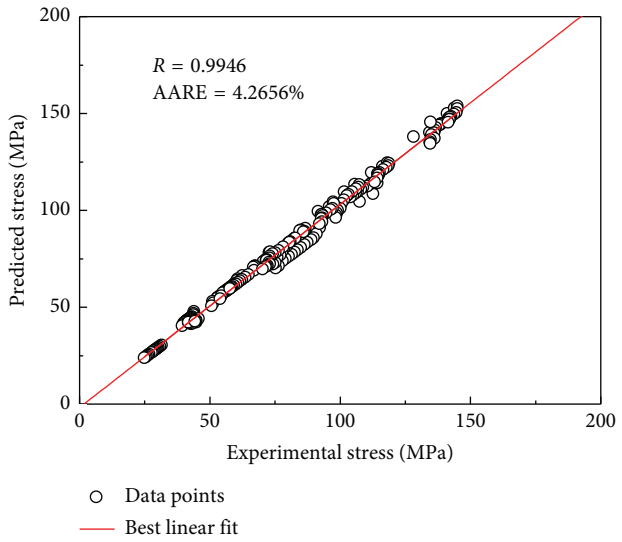

Figure 6: Correlation between the experimental and the predicted flow stress from the constitutive models based on orthogonal analysis for the AA6061 alloy under PSC.

between the strain rate and temperature on the stress can be neglected when compared with the individual effect of the strain rate and temperature. The strain-compensated constitutive model based on orthogonal analysis is developed, and the activation energy Q is found to be 158.465 kJ/mol.

(3) The correlation coefficient and the average absolute relative error between the experimental and the predicted flow stress by the developed models are 0.9946 and 4.2656%, respectively. Thus, the developed constitutive models based on orthogonal analysis can be used to predict the flow stress precisely at a wide range of strains, strain rates, and temperatures.

Data Availability

We confirmed that the experimental data used to support the findings of this study are included within the article.

Conflicts of Interest

The authors declare that there are no conflicts of interest regarding the publication of this paper.

Acknowledgments

This work was supported by the Innovation Project of Guangdong Academy of Sciences (No. 2018GDASCX-0965), the National Natural Science Foundation of China (Nos. 51575371 and 51875383), the Natural Science Foundation of Guangxi (No. 2018GXNSFBA281056), the Foundation of Guilin University of Technology (No. GUTQDJJ2017140), and the Science and Technology Major Project of Guangxi (No. GKAA17202007).

References

[1] F. Ozturk, A. Sisman, S. Toros, S. Kilic, and R. C. Picu, "Influence of aging treatment on mechanical properties of 6061 aluminum alloy," *Materials & Design*, vol. 31, no. 2, pp. 972–975, 2010.

[2] W. S. Lee, J. C. Shyu, and S. T. Chiou, "Effect of strain rate on impact response and dislocation substructure of 6061-T6 aluminum alloy," *Scripta Materialia*, vol. 42, no. 1, pp. 51–56, 2000.

[3] U. M. Iqbal and V. S. S. Kumar, "An analysis on effect of multipass twist extrusion process of AA6061 alloy," *Materials & Design*, vol. 50, pp. 946–953, 2013.

[4] N. Anjami and A. Basti, "Investigation of rolls size effects on hot ring rolling process by coupled thermo-mechanical 3D-FEA," *Journal of Materials Processing Technology*, vol. 210, no. 10, pp. 1364–1377, 2010.

[5] H. Yang, M. Wang, L. G. Guo, and Z. C. Sun, "3D coupled thermo-mechanical FE modeling of blank size effects on the uniformity of strain and temperature distributions during hot rolling of titanium alloy large rings," *Computational Materials Science*, vol. 44, no. 2, pp. 611–621, 2008.

[6] F.-C. Qin, Y.-T. Li, H.-P. Qi, and L. Ju, "Microstructure-Texture-mechanical properties in hot rolling of a centrifugal casting ring blank," *Journal of Materials Engineering and Performance*, vol. 25, no. 3, pp. 1237–1248, 2016.

[7] L. D. Pari Jr. and W. Z. Misiolek, "Theoretical predictions and experimental verification of surface grain structure evolution for AA6061 during hot rolling," *Acta Materialia*, vol. 56, no. 20, pp. 6174–6185, 2008.

[8] L. Cheng, X. Xue, B. Tang et al., "Deformation behavior of hot-rolled IN718 superalloy under plane strain compression at elevated temperature," *Materials Science and Engineering: A*, vol. 606, pp. 24–30, 2014.

[9] N. Bontcheva, G. Petzov, and L. Parashkevova, "Thermo-mechanical modelling of hot extrusion of Al-alloys, followed by cooling on the press," *Computational Materials Science*, vol. 38, no. 1, pp. 83–89, 2006.

[10] H. Grass, C. Krempaszky, and E. Werner, "3-D FEM-simulation of hot forming processes for the production of a connecting rod," *Computational Materials Science*, vol. 36, no. 4, pp. 480–489, 2006.

[11] M. Xiao, F. Li, W. Zhao, and G. Yang, "Constitutive equation for elevated temperature flow behavior of TiNiNb alloy based on orthogonal analysis," *Materials & Design*, vol. 35, pp. 184–193, 2012.

[12] D. Samantaray, S. Mandal, and A. K. Bhaduri, "A comparative study on Johnson Cook, modified Zerilli-Armstrong and Arrhenius-type constitutive models to predict elevated temperature flow behaviour in modified 9Cr-1Mo steel," *Computational Materials Science*, vol. 47, no. 2, pp. 568–576, 2009.

[13] J. Cheng and S. Nemat-Nasser, "A model for experimentally-observed high-strain-rate dynamic strain aging in titanium," *Acta Materialia*, vol. 48, no. 12, pp. 3131–3144, 2000.

[14] H. J. McQueen and N. D. Ryan, "Constitutive analysis in hot working," *Materials Science and Engineering: A*, vol. 322, no. 1-2, pp. 43–63, 2002.

[15] S. Mandal, V. Rakesh, P. V. Sivaprasad, S. Venugopal, and K. V. Kasiviswanathan, "Constitutive equations to predict high temperature flow stress in a Ti-modified austenitic stainless steel," *Materials Science and Engineering: A*, vol. 500, no. 1-2, pp. 114–121, 2009.

[16] Y. C. Lin and X.-M. Chen, "A critical review of experimental results and constitutive descriptions for metals and alloys in hot working," *Materials & Design*, vol. 32, no. 4, pp. 1733–1759, 2011.

[17] H. Mirzadeh, M. H. Parsa, and D. Ohadi, "Hot deformation behavior of austenitic stainless steel for a wide range of initial grain size," *Materials Science and Engineering: A*, vol. 569, pp. 54–60, 2013.

[18] W. Peng, W. Zeng, Q. Wang, and H. Yu, "Comparative study on constitutive relationship of as-cast Ti60 titanium alloy during hot deformation based on Arrhenius-type and artificial neural network models," *Materials & Design*, vol. 51, pp. 95–104, 2013.

[19] J. Liu, W. Zeng, Y. Lai, and Z. Jia, "Constitutive model of Ti17 titanium alloy with lamellar-type initial microstructure during hot deformation based on orthogonal analysis," *Materials Science and Engineering: A*, vol. 597, pp. 387–394, 2014.

[20] J. Cai, Y. Lei, K. Wang, X. Zhang, C. Miao, and W. Li, "A comparative investigation on the capability of modified Zerilli-Armstrong and Arrhenius-type constitutive models to describe flow behavior of $BFe_{10\text{-}1\text{-}2}$ cupronickel alloy at elevated temperature," *Journal of Materials Engineering and Performance*, vol. 25, no. 5, pp. 1952–1963, 2016.

[21] Y.-C. Lin, M.-S. Chen, and J. Zhang, "Modeling of flow stress of 42CrMo steel under hot compression," *Materials Science and Engineering: A*, vol. 499, no. 1-2, pp. 88–92, 2009.

[22] D. Samantaray, S. Mandal, and A. K. Bhaduri, "Constitutive analysis to predict high-temperature flow stress in modified 9Cr-1Mo (P91) steel," *Materials & Design*, vol. 31, no. 2, pp. 981–984, 2010.

[23] H. R. Ezatpour, M. Haddad Sabzevar, S. A. Sajjadi, and Y. Huang, "Investigation of work softening mechanisms and texture in a hot deformed 6061 aluminum alloy at high temperature," *Materials Science and Engineering: A*, vol. 606, pp. 240–247, 2014.

[24] A. Dorbane, G. Ayoub, B. Mansoor, R. Hamade, G. Kridli, and A. Imad, "Observations of the mechanical response and evolution of damage of AA 6061-T6 under different strain rates and temperatures," *Materials Science and Engineering: A*, vol. 624, pp. 239–249, 2015.

[25] T. Pettersen and E. Nes, "Recrystallization of an AlMgSi alloy after different modes of hot deformation," *Metallurgical and Materials Transactions A*, vol. 34, no. 12, pp. 2717–2726, 2003.

[26] G. Xiao, Q. Yang, L. Li, and J. Zeng, "Constitutive analysis of 6013 aluminum alloy in hot plane strain compression process considering deformation heating integrated with heat transfer," *Metals and Materials International*, vol. 22, no. 1, pp. 58–68, 2016.

[27] F. Qin, H. Qi, and Y. Li, "A comparative study of constitutive characteristics and microstructure evolution between uniaxial and plane strain compression of an AA6061 alloy," *Journal of Materials Engineering and Performance*, vol. 28, no. 6, pp. 3487–3497, 2019.

[28] Y. C. Lin, F.-Q. Nong, X.-M. Chen, D.-D. Chen, and M.-S. Chen, "Microstructural evolution and constitutive models to predict hot deformation behaviors of a Nickel-based superalloy," *Vacuum*, vol. 137, pp. 104–114, 2017.

[29] D.-D. Chen, Y. C. Lin, Y. Zhou, M.-S. Chen, and D.-X. Wen, "Dislocation substructures evolution and an adaptive-network-based fuzzy inference system model for constitutive behavior of a Ni-based superalloy during hot deformation," *Journal of Alloys and Compounds*, vol. 708, pp. 938–946, 2017.

[30] Q. Qin, Y. Tan, Z. Zhang, Q. Wang, and Y. Yang, "Effects of homogenization on hot deformation behavior of as-cast Mg-8Gd-3Y-1Nd-0.5Zr magnesium alloy," *Journal of Materials Engineering and Performance*, vol. 25, no. 1, pp. 304–311, 2016.

[31] C. M. Sellars and W. J. McTegart, "On the mechanism of hot deformation," *Acta Metallurgica*, vol. 14, no. 9, pp. 1136–1138, 1966.

[32] E. Cerri, E. Evangelista, A. Forcellese, and H. J. McQueen, "Comparative hot workability of 7012 and 7075 alloys after different pretreatments," *Materials Science and Engineering: A*, vol. 197, no. 2, pp. 181–198, 1995.

[33] Y.-X. Liu, Y. C. Lin, and Y. Zhou, "2D cellular automaton simulation of hot deformation behavior in a Ni-based superalloy under varying thermal-mechanical conditions," *Materials Science and Engineering: A*, vol. 691, pp. 88–99, 2017.

[34] S. Chen, K. Chen, G. Peng, X. Chen, and Q. Ceng, "Effect of heat treatment on hot deformation behavior and microstructure evolution of 7085 aluminum alloy," *Journal of Alloys and Compounds*, vol. 537, pp. 338–345, 2012.

[35] S. Liu, J. You, X. Zhang, Y. Deng, and Y. Yuan, "Influence of cooling rate after homogenization on the flow behavior of aluminum alloy 7050 under hot compression," *Materials Science and Engineering: A*, vol. 527, no. 4-5, pp. 1200–1205, 2010.

[36] J. Zhang, B. Chen, and Z. Baoxiang, "Effect of initial microstructure on the hot compression deformation behavior of a 2219 aluminum alloy," *Materials & Design*, vol. 34, pp. 15–21, 2012.

[37] S. Spigarelli, E. Evangelista, and H. J. McQueen, "Study of hot workability of a heat treated AA6082 aluminum alloy," *Scripta Materialia*, vol. 49, no. 2, pp. 179–183, 2003.

[38] C.-L. Gan, K.-H. Zheng, W.-J. Qi, and M.-J. Wang, "Constitutive equations for high temperature flow stress prediction of 6063 Al alloy considering compensation of strain," *Transactions of Nonferrous Metals Society of China*, vol. 24, no. 11, pp. 3486–3491, 2014.

[39] F. J. Li, Y. W. Zhai, X. Bian, and Z. P. Zhong, "Study of plastic deformation behavior on 6061 aluminum alloy," *Journal of Plasticity Engineering*, vol. 22, no. 2, pp. 95–99, 2015, in Chinese.

[40] X. L. Zhao, J. S. Qiao, and J. H. Chen, "Hot compression behavior of 6061 aluminum alloy," *Hot Working Technology*, vol. 38, no. 2, pp. 10–12, 2009, in Chinese.

[41] N. Kotkunde, H. N. Krishnamurthy, P. Puranik, A. K. Gupta, and S. K. Singh, "Microstructure study and constitutive modeling of Ti-6Al-4V alloy at elevated temperatures," *Materials & Design (1980–2015)*, vol. 54, pp. 96–103, 2014.

[42] M. Detrois, R. C. Helmink, and S. Tin, "Hot deformation characteristics of a polycrystalline γ-γ'-δ ternary eutectic Ni-base superalloy," *Materials Science and Engineering: A*, vol. 586, pp. 236–244, 2013.

[43] M. Morakabati, M. Aboutalebi, S. Kheirandish, A. Karimi Taheri, and S. M. Abbasi, "High temperature deformation and processing map of a NiTi intermetallic alloy," *Intermetallics*, vol. 19, no. 10, pp. 1399–1404, 2011.

[44] J. Zhao, H. Ding, W. Zhao, M. Huang, D. Wei, and Z. Jiang, "Modelling of the hot deformation behaviour of a titanium alloy using constitutive equations and artificial neural network," *Computational Materials Science*, vol. 92, pp. 47–56, 2014.


The Scientific
World Journal
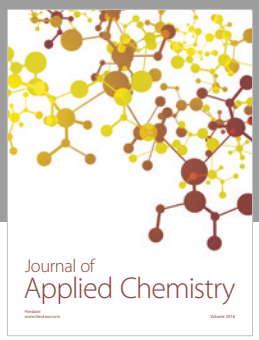
Journal of
Applied Chemistry
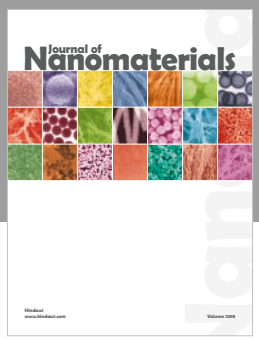
Journal of
Nanomaterials

Scientifica

International Journal of
Polymer Science
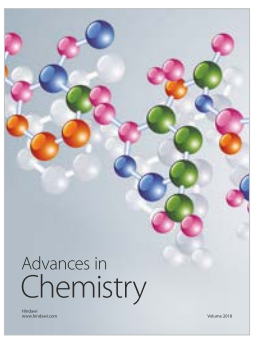
Advances in
Chemistry

Hindawi
Submit your manuscripts at
www.hindawi.com
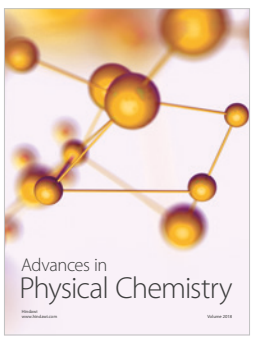
Advances in
Physical Chemistry

International Journal of
Analytical Chemistry
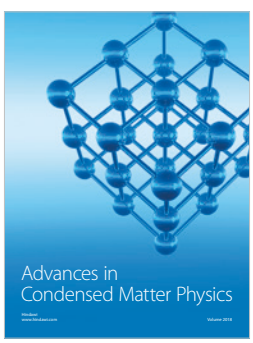
Advances in
Condensed Matter Physics
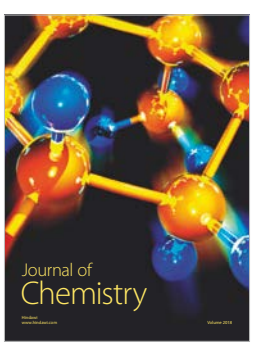
Journal of
Chemistry

International Journal of
Biomaterials
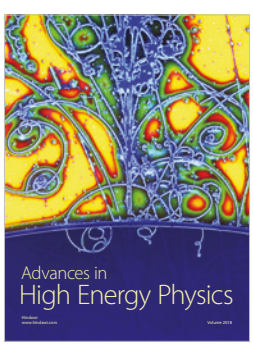
Advances in
High Energy Physics

Journal of
Engineering

Journal of
Nanotechnology

International Journal of
Corrosion

Journal of
Materials

BioMed
Research International
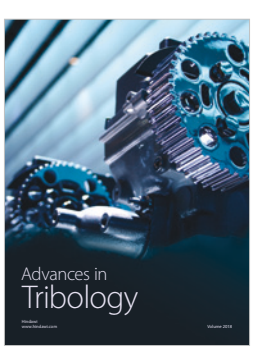
Advances in
Tribology
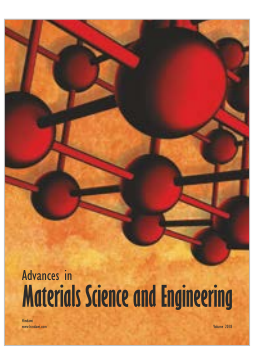
Advances in
Materials Science and Engineering